Application of f k Analysis and Entropy to Track the Transition from Spatially Coherent to Incoherent Earthquake Coda in Long Beach, California

Luis A. Domínguez, Paul M. Davis, and Dan Hollis

March 7, 2014

Published "Seismological Research Letters Volume 84, Number 4 July/August 2013"

Abstract:

Seismic-scattering theories describe high-frequency coda waves as a combination of waves from random scatterers superimposed on direct waves from the source. The direct waves are expected to be spatially coherent whereas the scattered waves, arriving with random phase, will be spatially incoherent. Our objective is to use data from an extreme high-resolution seismic experiment in Long Beach, California, to determine the transition from coherent to incoherent coda. The network, deployed by Nodal Seismic, comprises 5400 vertical component instruments, spaced every 100 m over an area of 5×7 km2. It was deployed for a period of six months with the primarily target to image the geological structure of the area for oil exploration. During the deployment, several thousand earthquakes and microearthquakes were recorded. We examine coda waves from the two largest events that occurred in the vicinity of the array.We compute frequency–wavenumber diagrams to determine the sources of coda and their evolution in time. Entropy analysis of the propagation of seismic waves through the array indicates the transition between the coherent direct body waves and the onset of incoherent coda waves. Our analysis illustrates that after the arrival of the body waves, the seismic coda is initially dominated by a dispersing wave train composed of spatially coherent body waves, forward scattered from 1D crustal layering.

This is then followed by omni-directional, spatially incoherent coda waves that can be described as scattered waves from 3D random sources.

INTRODUCTION

Pioneering work by Aki (1969) first recognized that coda is the result of scattering due to the random distribution of heterogeneities in the crust. In later work, Aki and Chouet (1975) developed a theoretical model of single scattering, using the Born approximation, that fits observations of energy decay of coda. Rautian and Khalturin (1978) recognized that the the Born approximation, that fits observations of energy decay of coda. Rautian and Khalturin (1978) recognized that the early portion of the coda is different at nearby stations, but nearby stations obtain a common envelope for times greater than twice the lapse time. Single-scattering models assume that the mean free path is greater than the distance between the scatterer and the receiver. Recognition that for long lapse times multi-scattering may be important, led to the development of multiple-scattering models. Dainty and Toksöz (1981) proposed a continuum model of scattering using the diffusion equation; this model explains the slow decay observed in records of lunar impacts. Frankel and Clayton (1986) introduced an energy-flux model corroborated by 2D finite-difference simulations. Wu and Aki (1985) and Zeng (1993) developed a model based on the radiative transfer theory. Margerin et al. (2009) suggested a rapid transition to the diffusion regime after the S-wave arrival. Although all models give similar results, they have in common that the S wave is followed by scattered energy from random sources. The scattered energy is either explicitly or implicitly random in space and time. We test this assumption here.

DATA

We analyzed the vertical component seismic records from two local events. The first event occurred on Friday, 13 May 2011 at 9:19:00 PM (Local Time), in the city of Carson (hereafter Carson Event) □ 8 km west of the seismic array. The magnitude and depth reported by USGS are Mw 2.5 and 10 km, respectively. The second event occurred □ 15 km northwest of the network on Monday, 6 June 2011 at 0:09:10 a.m. (Local Time) in the city of Compton (hereafter Compton event). The magnitude and depth reported by USGS are Mw 3.4 and 24.4 km, respectively. The Carson event is one order of magnitude smaller than the Compton event and occurred at a quieter time, Friday night. In both cases, urban noise is clearly observed. Additionally, each event had significant differences in depth (10 and 24 km). Therefore, they can be used to examine effects of the crustal structure and near-surface effects caused by faulting

and layering. The number of stations processed in each analysis varies between □ 150–5000 according to the frequency of interest. Figure 1 shows the location of the stations and the events analyzed.

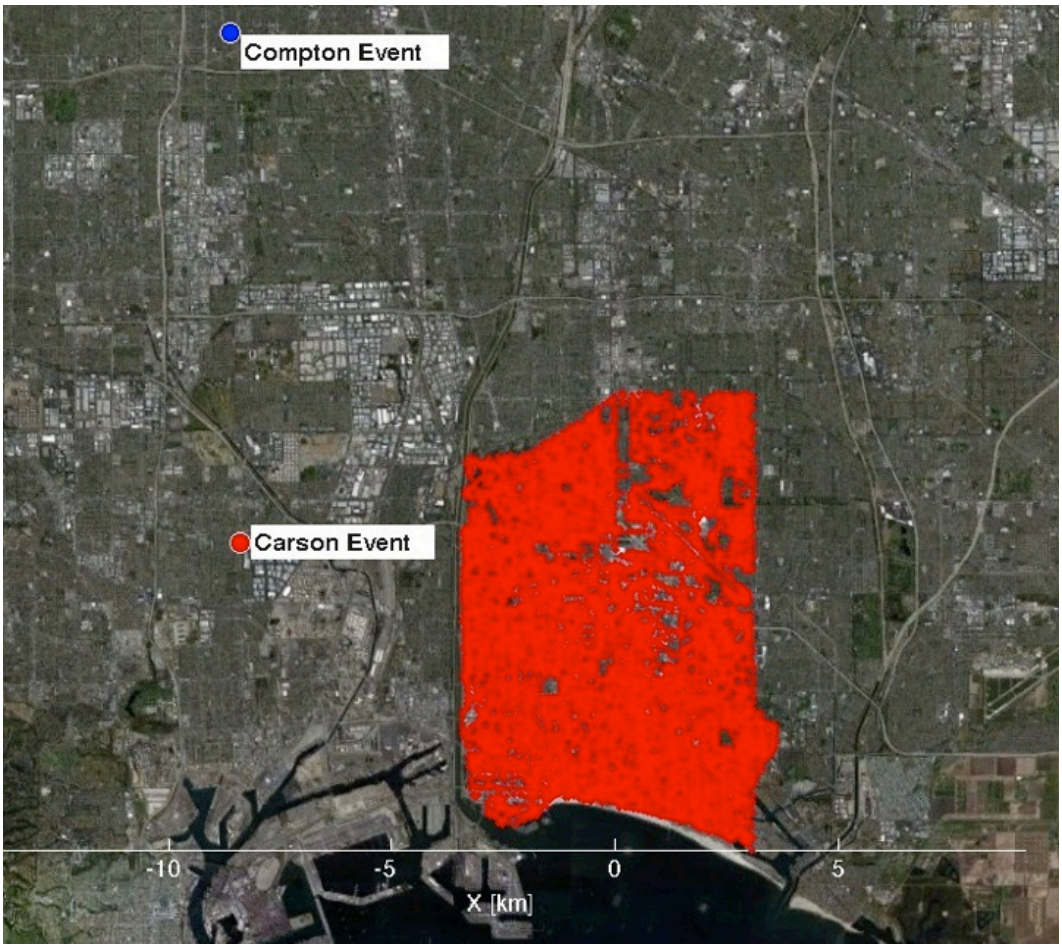

Figure 1: 1. Location of the stations deployed in Long Beach (white dots) and the M_w 2.5 Carson event and the M_w 3.4 Compton event.

f k ANALYSIS

The frequency–wavenumber f k analysis (e.g., Rost and Thomas [2002]) is used to determine the orientation and apparent slowness of the incident field. This technique consists in stacking band-passed seismic records at different reduced times depending

on the relative location of the station over a range of values of apparent slowness and azimuth. The stacked signal is calculated as:

$$y(t) = \frac{1}{N}\sum_{n=1}^{N} x_n(t - \bar{u}.\bar{r}_n). \quad (1)$$

N is the total number of seismogram (stations), and n is the receiver index. r_n is the relative location of the stations, where the origin is set to the center of the array. u is the apparent slowness, $u = frac1v(cos\psi, -sin\psi)$, , where v is the apparent velocity and ψ is the azimuth. The amplitude of the stacked signal y_t is at maximum when the individual records align coherently for a specific pair (v, ψ) . Stacking is carried out in a 3 s window to examine the time variation of the seismic wave field. The energy of the stacked signal is computed as:

$$E(t) = \int_{t}^{t+D} y^2(t)dt, \quad (2)$$

where D is the width of the time window.

Two strong signals are observed in the f k analysis for the Compton event at 6.60 s (Fig. 2) interpreted as a direct and a scattered wave (the energy is plotted as a function of horizontal apparent velocity rather than slowness to give beamforming diagrams). A scattered signal is clearly seen in the frequency bands 1–2, and 2–4 Hz. The stronger direct arrival detected shows an apparent velocity of 8 km/s and an azimuth of 300°. The secondary wave appears slightly later in time with a slower apparent velocity 5 km/s and azimuth 320°. The first signal corresponds to the arrival of the S waves; the secondary phase is likely due to the existence of a structure that diffracted a significant part of the direct energy. Structures associated with the Newport–Inglewood fault or the Los Angeles basin could conceivably cause such multipathing. A similar anomalous signal is not observed for the Carson event (see Fig. 3). In both cases the transition between direct and coda waves occurs within a few seconds after the arrival of the S wave, as suggested by the entropy analysis described in the next section, and so a scattered phase might be obscured by the coda waves.

ENTROPY ANALYSIS

Entropy is often used to quantify the randomness of a system. Thanks to the high spatial density of the network, it is possible to analyze the entropy transitions of the network as the seismic wave field propagates through it. When all stations see a coherent waveform, entropy will have minimum values. In contrast, when scattered waves

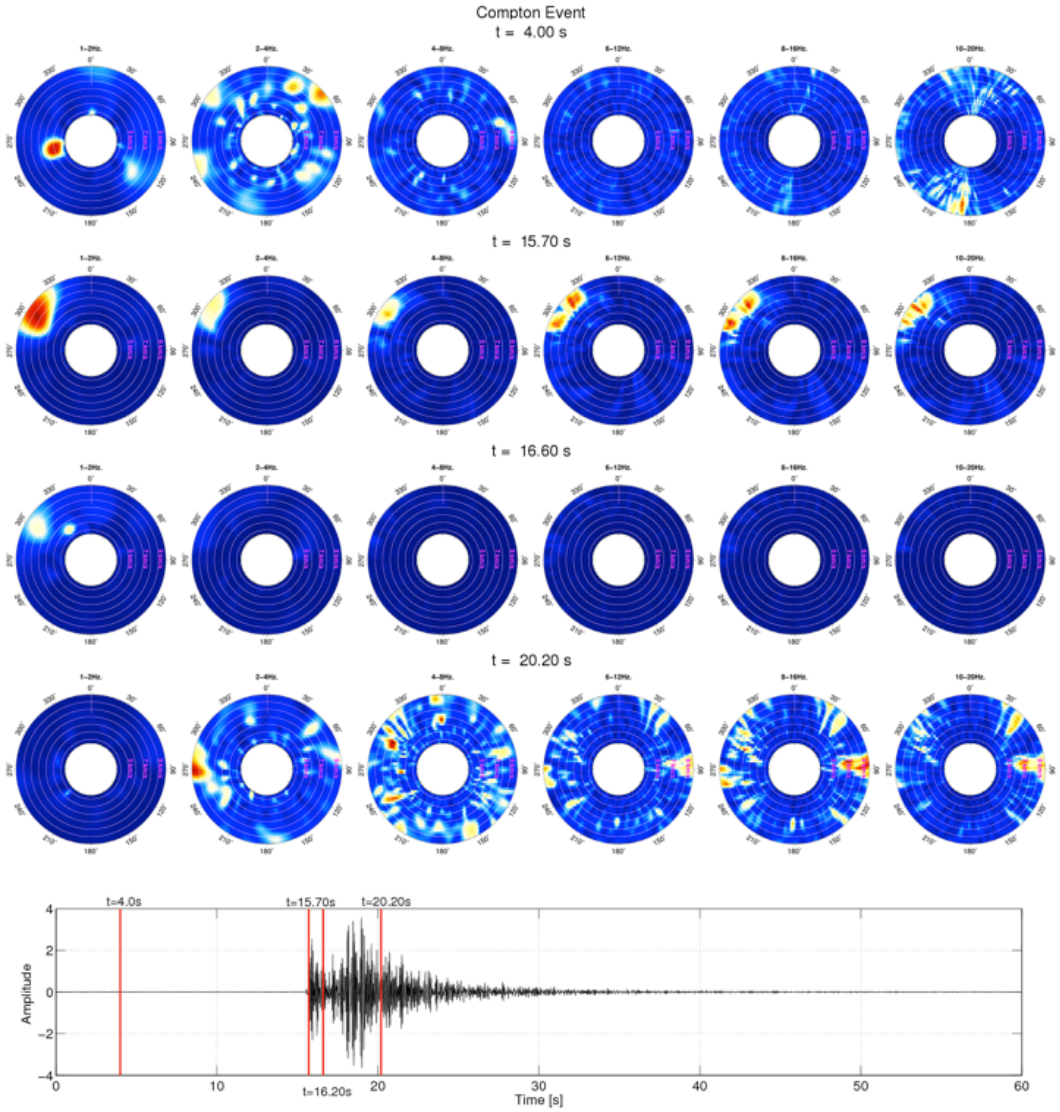

Figure 2: (a) Beamforming diagrams for the Compton event. Rows show snapshots at constant time for different frequencies (columns). (b) Sample seismogram for a station located roughly in the middle of the array indicating the times at which the diagram is computed.

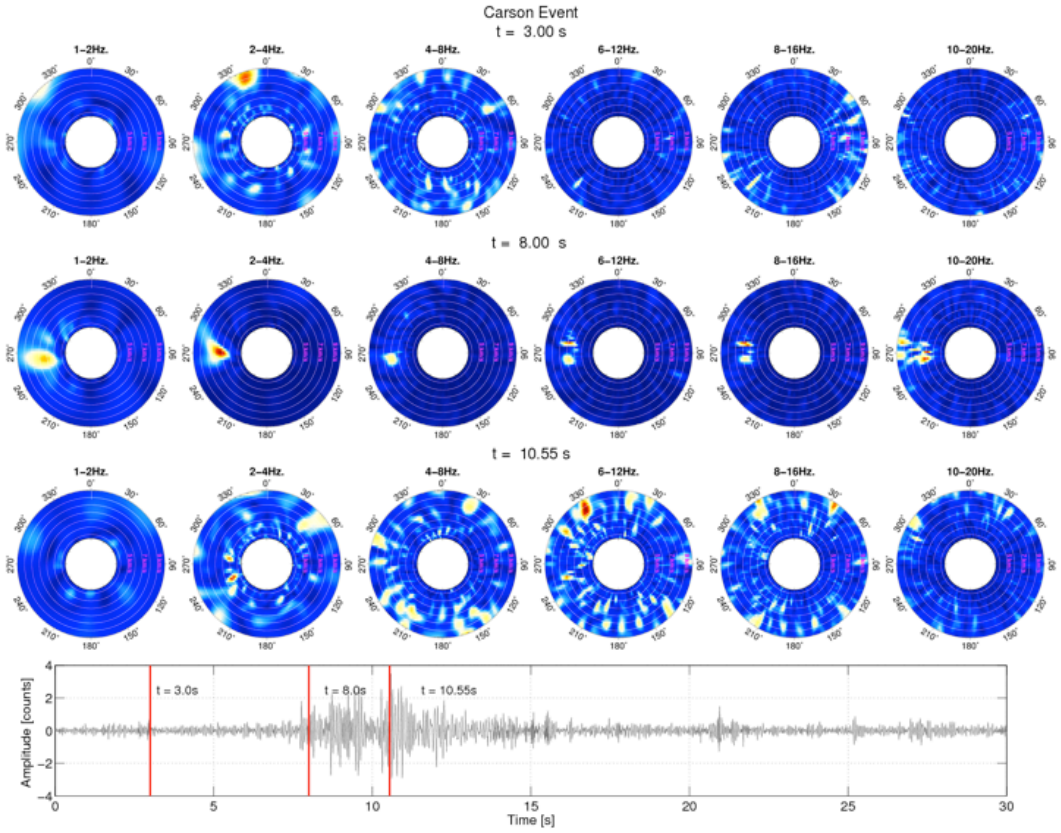

Figure 3: (a) Beamforming diagrams for the Carson event. Rows show snapshots at constant time for different frequencies (columns). (b) Sample seismogram for a station located roughly in the middle of the array indicating the times at which the diagram is computed.

or noise arise from many directions entropy reaches maximum levels. We use the definition of entropy as stated in information theory (Shannon, 1948),

$$H(x) = -\sum_{i=1}^{n} p_i(x_i) log_b(x_i), \tag{3}$$

where x is the state and $p(x)$ is the probability of a given state. Entropy is at maximum when all states are equally probable. Seismograms are discrete representations of the velocity of the wave field as a function of time. In order to explore the entropy of the network, we consider two possible states $n = 2$ of the seismograms, that is, they are either positive or negative (the zero state is neglected). We are thus testing for phase coherence ignoring amplitudes. If the wave field is coherent, closely spaced adjacent stations should be equally positive or negative. We test this by random sampling of the network by subarrays of two or more stations and averaging the entropy of each. Let the subarrays have characteristic size $L = 2\alpha\lambda$.We choose $\alpha = 0.5$ in order to have enough stations reporting for the highest frequency (15 Hz). For each subarray we calculate p1 is the (number of positive signals)/(number of stations) and p2 is the (number of negative signals)/(number of stations). Then,

$$H(x) = -p_1(x) ln(p_1(x)) - p_2(x) ln(P_2(x)) \tag{4}$$

For example, if the signals are spatially random on average, half will be positive and half negative. Entropy is then maximum $H(x) = 0.6931$. If on the other hand they are spatially uniform, that is, the amplitudes are all positive or all negative, the entropy $H(x)_{\alpha\rightarrow=0}$. This limit is not reached because $\square$ is necessarily finite, and so some subarrays will span zero crossings with positives and negatives on either side. The effect of finite $\square$ can be calculated by integrating equations (3) and (4) for cases where the subarrays overlap zero crossings. The effect is to raise the entropy floor by a value equal to α (see Appendix A). Nonetheless, by fixing α, relative entropies at different frequencies can be compared.

Figure 4 shows the entropy–energy analysis for the Compton event in the band 1–4 Hz (central frequency 3 Hz). Figure 4a shows the map of the stations and the classification of the stations. Black circles indicate what we define as central stations; gray circles are neighbor stations in a radius of $R_m < L/2 = \alpha\lambda$ from the central station; and open circles are stations not used in this calculation. Each neighborhood has a range of 1–16 stations. Then we determine the entropy by estimating the probability of each state, by counting the number of positive or negative states to obtain p_1 and p_2, respectively, and dividing by the number of stations in the neighborhood. This calculation is repeated in each neighborhood and then averaged for the entire array. Figure

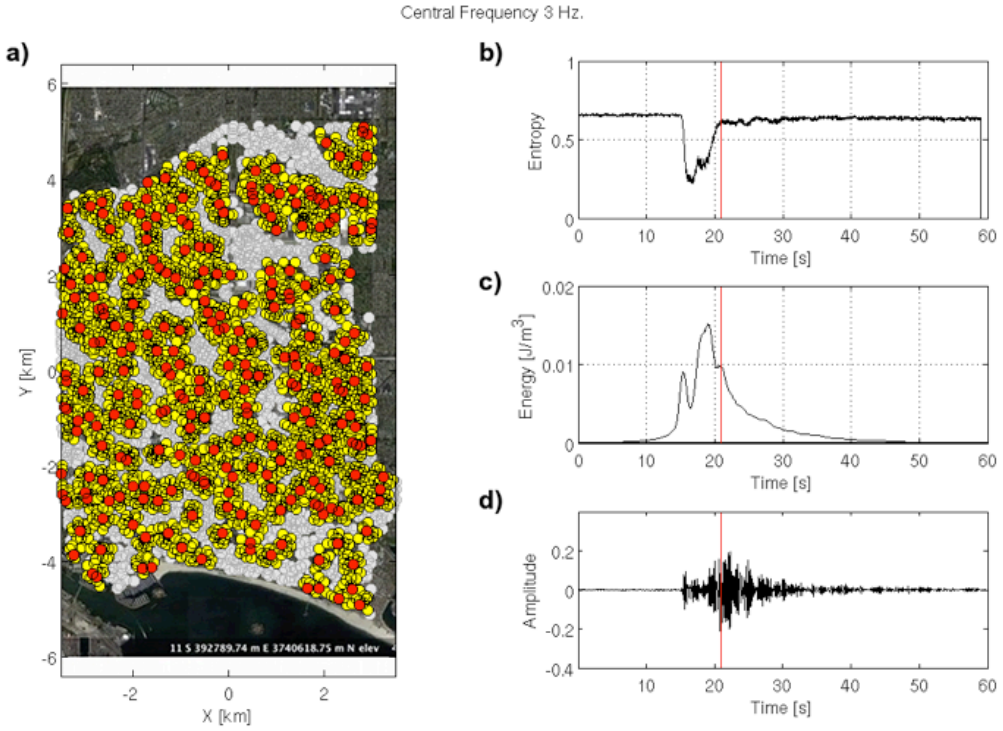

Figure 4: Entropy–energy analysis. (a) Map and classification of the stations. Red circles mark the central stations; yellow circles indicate the neighbor stations of size $L = \alpha\lambda$; and open circles denote stations not used in this computation; (b) normalized entropy decay; (c) average energy computed using equation (2); and (d) sample seismogram randomly chosen from the network. The solid line marks the transition from coherent arrivals to noise-like random state.

4b–d shows the entropy, the average energy, and a randomly chosen sample seismogram, respectively. Figure 5 shows the entropy analysis at different frequencies: 1.5, 3.0, 6.0, 9.0, 12.0, and 15Hz for both events where we have normalized the entropy at the noise level to 1. The number of stations used at each calculation decreases for high frequencies. The most interesting result lies in the fact that the entropy quickly recovers and fully stabilizes well before twice the lapse time for a constant L=□ . This marks the transition point at which seismic waves become incoherent and the beginning of random coda waves. It occurs when the energy levels are still well above the noise levels, whereas the entropy levels of noise and coda become indistinguishable. This observation is reproducible for both events despite the fact that the Carson event is one order of magnitude smaller than the Compton event.

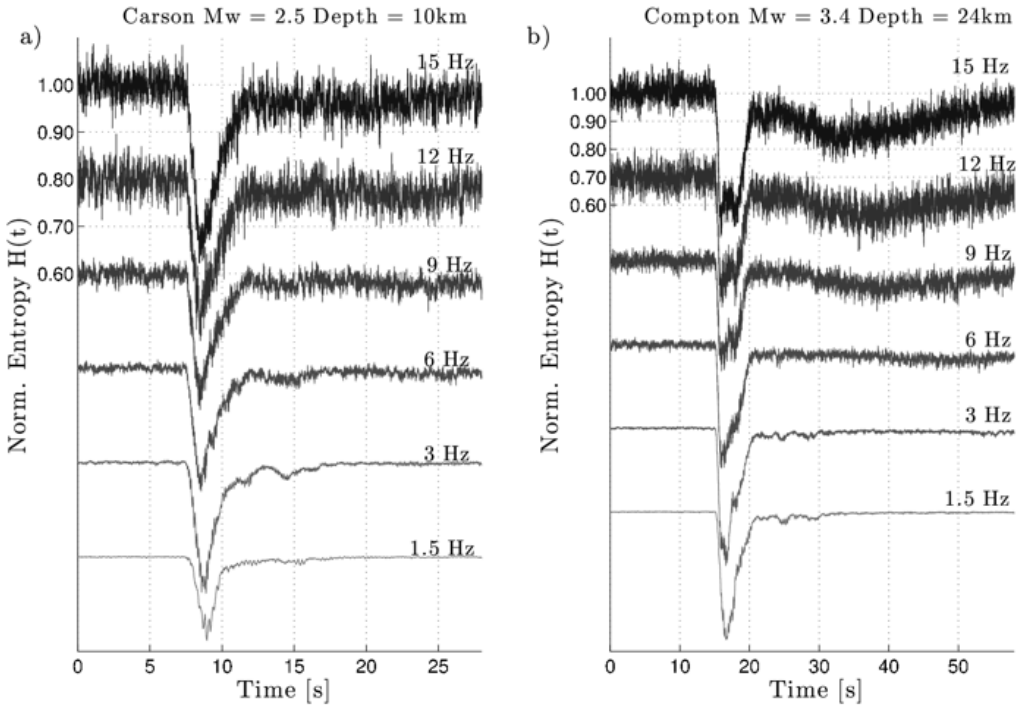

Figure 5: Entropy as a function of time for different frequency bands. (a) Carson event, and (b) Compton event. The frequency bands overlap each other, and so each frequency band is shifted vertically to make the variation clearer.

CONCLUSIONS

Analysis of the data from a dense seismic array in Long Beach suggests that the wave field reaches a disorder regime seconds after the S-wave arrival, at which isotropic scattering becomes the major contributor to the coda wave field. The f k diagrams show the distribution and evolution in time of the incoming energy at frequencies $1 \le f \le 20$ Hz. Shortly after the passage of the P and S waves, body waves lose their coherency and incoherent coda waves take over the spectrum. The beamforming diagrams of the Compton event show a strong secondary phase soon after the S-wave arrival at low frequencies $1 \le f \le 4$ Hz. This phase is likely due to the geometry of the basin and the fault zone north of the array. A similar phase is not observed for the Carson event suggesting a strong path effect that modifies the northwest–southeast trajectory. Entropy–energy analysis reveals the transition point between direct coherent body waves and incoherent coda waves. Entropy is used as an indicator of the randomness of the wave field and coherency between nearby stations. A significant drop in entropy occurs when direct body phases propagate through the array. As coda waves build up, entropy returns to the level prior to the earthquake even though the energy contained in the coda wave field is significantly above the noise level.

ACKNOWLEDGMENTS

The authors would like to thank two anonymous reviewers for their careful revision and suggestions that considerably improved the manuscript and the interpretation of the results. This research was supported by the Southern California Earthquake Center (SCEC). SCEC is funded by NSF Cooperative Agreement EAR-0529922 and USGS Cooperative Agreement 07HQAG0008. The SCEC contribution number for this paper is 1643.

REFERENCES

Aki, K. (1969). Analysis of seismic coda of local earthquakes as scattered waves, J. Geophys. Res. 74, no. 2, 615–631.

Aki, K., and B. Chouet (1975). Origin of coda waves: Source, attenuation, and scattering effects, J. Geophys. Res. 80, no. 23, 3322–3342.

Dainty, A., and M. Toksöz (1981). Seismic codas on the Earth and the Moon: A comparison, Phys. Earth Planet. In. 26, no. 4, 250–260.

Frankel, A., and R. Clayton (1986). Finite-difference simulations of seismic scattering: Implications for the propagation of short-period seismic waves in the crust and models of crustal heterogeneity, J. Geophys. Res. B Solid Earth Planets 91, no. B6,

6465–6489.

Margerin, L., M. Campillo, B. A. Van Tiggelen, and R. Hennino (2009). Energy partition of seismic coda waves in layered media: Theory and application to Pinyon Flats Observatory, Geophys. J. Int. 177, no. 2, 571–585, doi: 10.1111/j.1365-246X.2008.04068.x

Rautian, T., and V. Khalturin (1978). The use of the coda for determination of the earthquake source spectrum, Bull. Seismol. Soc. Am. 68, no. 4, 923–948.

Rost, S., and C. Thomas (2002). Array seismology: Methods and applications, Rev. Geophys. 40, no. 3, 1008.

Shannon, C. E. (1948). A mathematical theory of communication, Bell Syst. Techn. J. 27, 379–423, 623–656.

Wu, R., and K. Aki (1985). Elastic wave scattering by a random medium and the small-scale inhomogeneities in the lithosphere, J. Geophys. Res. 90, no. B12, 10,261–10,273.

Zeng, Y. (1993). Theory of scattered P-wave and S-wave energy in a random isotropic scattering medium, Bull. Seismol. Soc. Am. 83, no. 4, 1264–1276.

APPENDIX A

EFFECT OF FINITE WINDOW ON ENTROPY

Figure 6: Schematic diagram for the analysis of a sign-bit cosine signal using a finite sliding time window.

Figure 6 shows a cosine wave of wavelength λ that has been converted to sign bit. The bottom box is the sampling window $0, l$. When the window lies completely within the wave, the entropy is zero. However, when it overlaps positive and negative values at the beginning, the middle left side and right side, and end, it integrates entropy. We integrate a single overlap as drawn and, by symmetry, multiply by 4 for the remaining cases. Then,

$$P_1 = (1/2 + x/l)$$
$$p_2 = (1/2 - x.l),$$
$$\delta E = \frac{4}{\lambda}\int_0^{l/2} \{(1/2 + x/l)log * 1/2 + x/l)$$
$$+ (1/2 - x/l)log(1/2 - x/l)dx = l/\lambda$$

That is, the effect of a finite window is to raise the estimated entropy of a sign-bit cosine wave from zero to $\delta E = l/\lambda$.

Luis A. Domínguez
Paul M. Davis
Department of Earth and Space Sciences
University of California, Los Angeles
3806 Geology Building
595 Charles Young Drive East
Los Angeles, California 90095 U.S.A.
ladominguez@ucla.edu

Dan Hollis
Nodal Seismic LLC
2201 East Willow Street
Suite D #183
Signal Hill, California 90755 U.S.A.
dan.hollis@nodalseismic.com

The intellectual merit and broader impacts (e.g. outreach activity) of the funded work.

For the first time coda from earthquakes recorded by an unaliased array of 5000 stations 100 m apart has been used to track the transition from coherent forward-scattered waves to incoherent back-scattered waves. Back-scattered waves are used for determining site effects as they are thought to be incident from multiple directions and so do not suffer defocusng/focusing effects or amplitude modulation from the radiation pattern of direct waves. However when this transitio occurs has perviously relied on theoretical syntheses. We use an entropy measure to detect this transition, which aoccurs at approximately twice the S wave lapse time.

Understanding scattering is important for estimating ground motions and and seismic hazard at high frequencies where it is unlikey we will have ether the computing power or the detailed structural information to construct determininstic waveforms, and so must rely on stochastic propertiesas categorized here.